

## RESEARCH ARTICLE

10.1002/2016JC011890

## Key Points:

- Patterns of alongcoast winds in the Beaufort Sea have shifted in recent years due to regional atmospheric centers of action
- Wind-driven transport of the shelfbreak jet and upwelling are enhanced in June and October when storms are stronger and longer-lasting
- Seasonal variation of cetacean occurrence near the shelfbreak jet is impacted by pack-ice cover and upwelling

## Correspondence to:

P. Lin,  
plinwho@gmail.com

## Citation:

Lin, P., R. S. Pickart, K. M. Stafford, G. W. K. Moore, D. J. Torres, F. Bahr, and J. Hu (2016), Seasonal variation of the Beaufort shelfbreak jet and its relationship to Arctic cetacean occurrence, *J. Geophys. Res. Oceans*, 121, 8434–8454, doi:10.1002/2016JC011890.

Received 16 APR 2016

Accepted 10 NOV 2016

Accepted article online 16 NOV 2016

Published online 2 DEC 2016

## Seasonal variation of the Beaufort shelfbreak jet and its relationship to Arctic cetacean occurrence

Peigen Lin<sup>1,2</sup>, Robert S. Pickart<sup>2</sup>, Kathleen M. Stafford<sup>3</sup>, G. W. K. Moore<sup>4</sup>, Daniel J. Torres<sup>2</sup>, Frank Bahr<sup>2</sup>, and Jianyu Hu<sup>1</sup>

<sup>1</sup>State Key Laboratory of Marine Environmental Science, College of Ocean and Earth Sciences, Xiamen University, Xiamen, China, <sup>2</sup>Woods Hole Oceanographic Institution, Woods Hole, Massachusetts, USA, <sup>3</sup>Applied Physics Laboratory, University of Washington, Seattle, Washington, USA, <sup>4</sup>Department of Physics, University of Toronto, Toronto, Ontario, Canada

**Abstract** Using mooring time series from September 2008 to August 2012, together with ancillary atmospheric and satellite data sets, we quantify the seasonal variations of the shelfbreak jet in the Alaskan Beaufort Sea and explore connections to the occurrences of bowhead and beluga whales. Wind patterns during the 4 year study period are different from the long-term climatological conditions that the spring-time peak in easterly winds shifted from May to June and the autumn peak was limited to October instead of extending farther into the fall. These changes were primarily due to the behavior of the two regional atmospheric centers of action, the Aleutian Low and Beaufort High. The volume transport of the shelfbreak jet, which peaks in the summer, was decomposed into a background (weak wind) component and a wind-driven component. The wind-driven component is correlated to the Pt. Barrow, AK alongcoast wind speed record although a more accurate prediction is obtained when considering the ice thickness at the mooring site. An upwelling index reveals that wind-driven upwelling is enhanced in June and October when storms are stronger and longer-lasting. The seasonal variation of Arctic cetacean occurrence is dominated by the eastward migration in spring, dictated by pack-ice patterns, and westward migration in fall, coincident with the autumn peak in shelfbreak upwelling intensity.

## 1. Introduction

The Alaskan Beaufort Sea is impacted by both Pacific-origin and Atlantic-origin waters. As a predominate source of nutrients and heat, Pacific water plays a major role in the functioning of the ecosystem of the western Arctic and influences ice melt in the region [Shimada *et al.*, 2006; Woodgate *et al.*, 2010]. Driven by the Arctic-North Pacific sea surface height difference, the Bering Strait inflow carries Pacific water into the Chukchi Sea [Aagaard *et al.*, 2006] and divides into several flow branches [Weingartner *et al.*, 2005]. In summer, a large portion of the inflowing Pacific water drains into the Canada Basin through Barrow Canyon [Itoh *et al.*, 2015; Gong and Pickart, 2015; Pickart *et al.*, 2016], much of it via the Alaskan Coastal Current (ACC) which flows northeastward along the Alaskan coast (Figure 1) [Paquette and Bourke, 1979; Weingartner *et al.*, 2005].

Some of the Pacific water that exits Barrow Canyon forms an eastward flowing current along the edge of the Alaskan Beaufort shelf, which is referred to as the Beaufort shelfbreak jet or the western Arctic boundary current [Nikolopoulos *et al.*, 2009]. The structure and transport of this current varies strongly with season. Using historical shipboard hydrographic data [Pickart, 2004] and data from a high-resolution mooring array [Nikolopoulos *et al.*, 2009; von Appen and Pickart, 2012], it was determined that during spring and early summer, the current is bottom-intensified and transports cold Pacific winter water. Then from midsummer to early fall, warm Pacific summer waters are advected eastward in a surface-intensified jet. During the remainder of the year the current is again bottom-intensified, with a deep-reaching “tail,” and transports modified summer and winter Pacific waters. Using subsequent data from a mooring deployed in the center of the current, Brugler *et al.* [2014] further quantified the seasonal variation of the Beaufort shelfbreak jet, and, in particular, characterized its volume, heat, and freshwater transport. They showed that the summer months (June through September) account for about 85% of the yearly volume transport of the current. Furthermore, they demonstrated that the transport of the current has dramatically decreased over the decade of the 2000s.

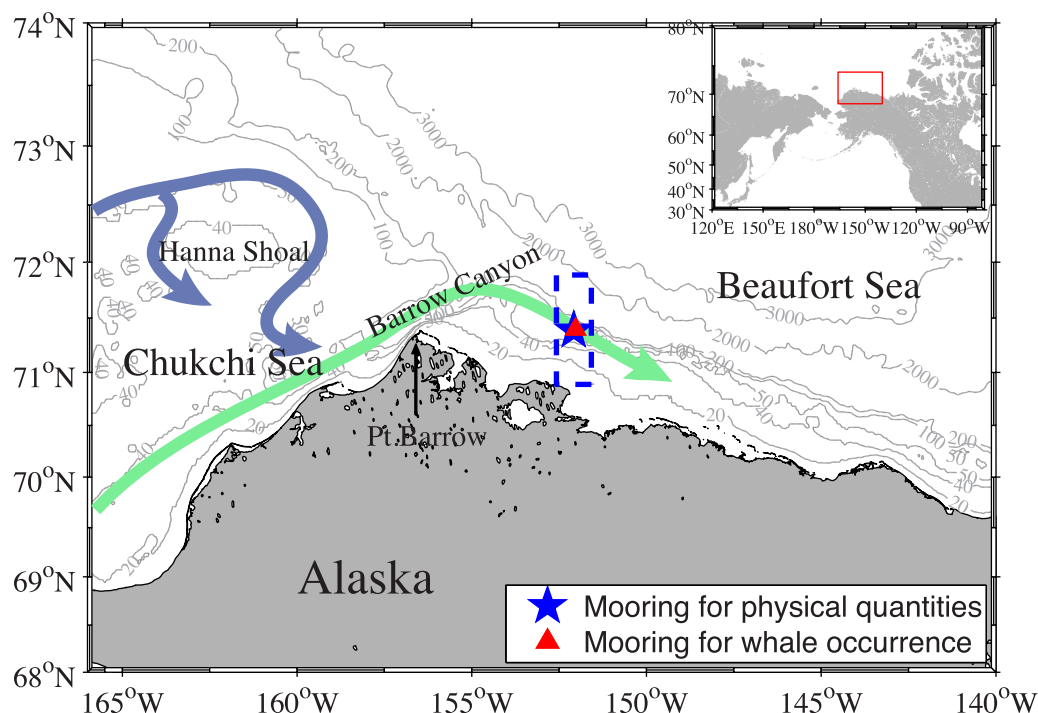


**Figure 1.** Location of the Arctic Observing Network (AON) physical mooring (blue star) and marine mammal passive acoustic mooring (red triangle). The blue dashed box ( $1^{\circ} \times 1^{\circ}$ ) is the region over which the ice concentration data are averaged. The arrows denote the major flow pathways of Pacific water entering Barrow Canyon and subsequently exiting the Chukchi Shelf: the green arrow is the ACC and the blue arrows are pathways on the central shelf. Bathymetric contours are in meters.

As discussed in many previous studies, the Pacific water consists of both summer waters and winter waters. The two predominant types of summer water are the Alaskan coastal water (ACW), which is relatively warm and fresh and transported northward through the Chukchi Sea by the ACC, and the Bering Summer water (BSW), which flows through the central/western side of Bering Strait and is commonly found in the central Chukchi shelf. (BSW is also referred to as Western Chukchi Summer water [Shimada *et al.*, 2001] and Chukchi Summer Water [von Appen and Pickart, 2012]). The two types of Pacific winter water are newly ventilated winter water (WW), which is fairly close to the freezing point, and older winter water that has been warmed via atmospheric heating and/or mixing subsequent to the winter season, referred to as remnant winter water (RWW).

Aagaard [1984] first described the subsurface circulation of warm Atlantic-origin water in the southern Canada Basin. This water flows eastward below roughly 180 m depth [Nikolopoulos *et al.*, 2009] as part of the large-scale cyclonic boundary current system of the Arctic Ocean [e.g., Rudels *et al.*, 2004; Karcher *et al.*, 2007]. Although the transport of the Atlantic water in the Canada Basin is presently unknown, part of it flows adjacent to the Pacific water on the Beaufort slope [Nikolopoulos *et al.*, 2009], and, during the winter months, it is accelerated as part of the spin-down phase of storm events [Pickart *et al.*, 2011].

Wind-driven upwelling is common in the Beaufort shelfbreak and can occur during all months of the year [e.g., Hufford, 1974; Pickart *et al.*, 2009; Schulze and Pickart, 2012]. The easterly winds that drive the upwelling are related to Pacific-born storms [Pickart *et al.*, 2009] as well as fluctuations of the Beaufort High [Watanabe, 2011]. As noted by Pickart *et al.* [2013b], the amount of salt fluxed onshore by a relatively small number of upwelling events is comparable to the vertical salt flux during polynya events, while the onshore nitrate flux could account for most of the net annual primary production on the Alaskan Beaufort shelf. The dynamics of the upwelling at the shelfbreak differ from that in canyons [e.g., Aagaard and Roach, 1990; Williams *et al.*, 2006]. Pickart *et al.* [2013b] demonstrated that Ekman theory accurately predicts the strength of shelfbreak upwelling in the Beaufort Sea and that the cross-stream flux of momentum is important in the depth-integrated alongstream force balance.

Sea ice plays an important role in the oceanographic processes in the Alaskan Beaufort Sea [e.g., Thorndike and Colony, 1982]. The pack-ice is forced by wind stress and also subject to internal ice stress, which is

proportional to the ice concentration [Røed and O'Brien, 1983]. Notably, even when the ice concentration is 100%, upwelling occurs at the shelfbreak during easterly wind events [Schulze and Pickart, 2012]. By constructing composite means, Schulze and Pickart [2012] found that the upwelling is strongest when there is partial ice cover. This is consistent with the results of Häkkinen [1986] who suggested that the air-ice momentum flux is greater than the air-ocean momentum flux, which in turn means that the Ekman transport should be larger under freely moving ice than in open water. In a numerical study, Martin *et al.* [2014] argued that the ocean response is strongest for an ice concentration of roughly 85%.

In the Alaskan Beaufort Sea there are two species of Arctic whales: belugas (*Delphinapterus leucas*) and bowheads (*Balaena mysticetus*). Belugas are typically observed over the outer-shelf and continental slope [Moore, 2000] and are comprised of two populations, the Eastern Chukchi Sea population and the Beaufort Sea population. While the two groups have different migratory timing and core use areas [Hauser *et al.*, 2014], their diets are similar, ranging from invertebrates to fish [Frost and Lowry, 1984; Loseto *et al.*, 2009; Quakenbush *et al.*, 2015]. Bowheads are the only Arctic endemic baleen whales, and they are uniquely adapted to live in the ice, although they feed in regions of open water. There is little information on how changing physical drivers affect Arctic marine mammals. However, the body condition (i.e., girth relative to length) of the western Arctic bowheads appears to be increasing, and this change is thought to be related to the decrease in summer sea ice and upwelling-driven increases in prey availability [George *et al.*, 2015].

The western Beaufort is a known hot spot for both species [Hauser *et al.*, 2014; Citta *et al.*, 2015]. However, at present it is poorly understood how bowheads and belugas rely on the oceanographic conditions along the Beaufort slope, and, in particular, the shelfbreak jet in terms of their habitat and feeding. In the Barrow Canyon region both species seem to take advantage of the presence of the ACC. When this current is well-established, beluga whales are believed to feed on prey accumulated by the associated hydrographic front [Stafford *et al.*, 2013]. In addition, upwelling in the canyon promotes the advection of zooplankton onto the shelf, and, when the winds relax, the reestablishment of the ACC "traps" euphausiids on the shelf where they provide food for migrating bowheads [Ashjian *et al.*, 2010; Okkonen *et al.*, 2011]. Since the summertime configuration of the Beaufort shelfbreak jet can be thought of as the eastward extension of the ACC and since upwelling is common along the Beaufort shelf/slope, it is likely that similar relationships exist there between the whales and the environmental conditions.

While the Beaufort shelfbreak jet has been extensively studied over the past decade, there remain open questions regarding the nature of its seasonal variability and whether or not this has changed over time. Furthermore, it remains to be determined how the physical attributes of the current might impact migrating cetaceans in the region. This paper uses mooring data from the Beaufort shelfbreak jet from September 2008 to August 2012, along with ancillary atmospheric and satellite information to quantify the seasonal patterns of flow, hydrography, winds, ice concentration and thickness, and cetacean occurrence. The reason why this 4 year period is chosen is that in addition to the physical measurements, we have contemporaneous time series from a passive acoustic recorder from the same location. We begin with a description of the mooring time series and the ancillary data used in the study. We then present a climatological seasonal cycle of different physical attributes of the current and the atmospheric forcing which reveals that, over the last decade, some of the seasonal trends have shifted. To address the cause of the seasonal shifts in the shelfbreak jet, we relate the variations to changes in the atmospheric centers of actions and local alongcoast wind. The latter is in turn used to predict the wind-driven transport of the shelfbreak jet by considering the effect of ice concentration. Finally, as a demonstration of the broader interdisciplinary applications of a long-term Arctic time series, we compute the analogous seasonal cycles of whale occurrence and explore some of the relationships between the presence of the Arctic cetaceans and environmental drivers.

## 2. Data and Methods

### 2.1. Physical Mooring Data

A yearlong mooring has been deployed in the center of the Beaufort shelfbreak jet, near 71°N, 152°W, as part of the Arctic Observing Network (AON) since August 2008 (Figure 1, blue star). The top float of the mooring is located at 35 m depth to avoid potential damage from ice keels. An upward facing RDI 75 kHz

acoustic Doppler current profiler (ADCP) with a vertical resolution of 10 m is situated at 128 m depth (roughly 20 m above the bottom) which samples hourly. (In 2009 to 2012 a second upward facing RDI 300 kHz ADCP with 5 or 10 m resolution was attached to the top float.) Hydrographic measurements between the top float and the lower ADCP (40–126 m) were made from a coastal moored profiler (CMP), which is a motorized conductivity-temperature-depth (CTD) instrument. This provided four vertical traces per day with a resolution of 2 m. Point CTD measurements were collected using two MicroCats, one attached to the top float and the other situated just below the deepest CMP depth. These data were used to help calibrate the CMP profiles following the procedure in *Fratantoni et al.* [2006]. The mooring also included an IPS-5 upward looking sonar on the top float to measure ice draft every 2 s. For more information about the instrumentation used on the mooring, including the calibration procedures and accuracy of the sensors, see *Spall et al.* [2008] and *Nikolopoulos et al.* [2009].

## 2.2. Whale Occurrence Data

Passive acoustic data were collected from an Aural-M2 instrument package deployed on a mooring located adjacent to the physical mooring, as part of the same AON project (Figure 1, red triangle). The instrument recorded from 10 to 4096 Hz (sample rate 8192 Hz, 2 byte resolution) on duty cycles that ranged from 9 to 10 min every 30 min. Data were archived within the instrument. Upon retrieval, spectrograms (frame size 2048 samples, 50% overlap, Hann window) of each acoustic data file were visually inspected for the presence of beluga and bowhead whale signals. The total number of files per day with at least one signal from each species was determined for the duration of the recordings and the climatological monthly mean was computed for the 4 years of data from September 2008 to August 2012 for both beluga and bowhead whales.

## 2.3. Meteorological Data

Wind data from 1950 to 2012 are used from the meteorological station at Pt. Barrow (Figure 1), obtained from National Climate Data Center (<http://www.ncdc.noaa.gov/>). This is the closest weather station to the mooring site. The data have been despiked and interpolated onto an hourly grid as outlined in *Pickart et al.* [2013a]. It has been previously demonstrated that the winds at this site are a good proxy for those at the mooring location [see *Nikolopoulos et al.*, 2009; *Pickart et al.*, 2009]. Following *Nikolopoulos et al.* [2009], we considered the wind speed in the alongcoast direction of 105°T. The long-term trend of the alongcoast wind speed was calculated using Singular Spectrum Analysis (SSA) low-frequency reconstruction [e.g., *Moore et al.*, 2012]. The nonparametric SSA is a method using data-adaptive functions to decompose a time series into statistically independent components [*Ghil et al.*, 2002]. The SSA transfers the original time series into a multidimensional matrix by sliding a window of length  $L$  in its decomposition stage. In this study we take  $L$  to be 12, which is one fifth of the wind time series length. Theoretically, it is acceptable if the window length is not greater than a half of the time series length [*Hassani*, 2007].

## 2.4. Atmospheric Reanalysis Data

Large-scale atmospheric fields are used to investigate the wind forcing at the mooring site. We employ sea-level pressure (SLP) and 10 m wind data from the North American Regional Reanalysis (NARR). This product combines the 2001 operational version of the National Centers for Environment Prediction (NCEP) regional Eta model and a data assimilation system [*Mesinger et al.*, 2006]. NARR has a temporal resolution of 6 h and spatial resolution of approximately 32 km. We consider the time period 1979–2012. The NARR fields have been used previously to document the characteristics and variation of the SLP and wind forcing in this region [e.g., *Brugler et al.*, 2014; *Spall et al.*, 2014], and there is good agreement between the NARR wind record and the measured winds at the Pt. Barrow meteorological station [*Pickart et al.*, 2011].

## 2.5. Ice Concentration Data

Two daily high-resolution sea ice concentration products were used in this study: (1) a blended data set that combines Advanced Very High Resolution Radiometer (AVHRR) and Advanced Microwave Scanning Radiometer (AMSR) fields for September 2008 to September 2011 and (2) a product using only AVHRR data for the period October 2011 to August 2012 (since the blended data set ended in September 2011). Both data sets have a spatial resolution of 0.25° and were adjusted using in situ data [*Reynolds et al.*, 2007]. The ice concentration was averaged within a 1° longitude by 1° latitude box centered around the mooring site (blue box in Figure 1).

### 3. Atmospheric Forcing

In a previous study using the Pt. Barrow meteorological station data, *Pickart et al.* [2013a] found that the climatological seasonal cycle of alongcoast wind speed contained two periods of enhanced easterly winds: one in spring (May) and the other in fall (October and November). This result is reproduced in Figure 2a, where the time period considered is September 1950 to August 2008. Computing the analogous seasonal cycle over the 4 year period of our study, September 2008 to August 2012, we find that there was a shift in these two periods of stronger winds (Figure 2b). Namely, the spring peak is now in June ( $>4 \text{ m s}^{-1}$ ), and the fall peak becomes shorter in duration, spanning only the month of October ( $\sim 3 \text{ m s}^{-1}$ ).

To investigate the nature of this change in the seasonal cycle, we considered the long-term variation (1950–2012) in wind speed for the spring and fall periods using the SSA algorithm described in section 2.3. Starting first with June, while there is considerable year to year variation for that month, there has been a trend of increasing easterly winds since the mid-1990s (Figure 3a). By contrast, there has been no such trend during the month of May (Figure 3b). In fact, the easterly alongcoast wind speed during that month tends to slowly decrease over the last 20 years. Consequently, by the end of the first decade of the 2000s, the easterly wind speed in June ( $\sim 4 \text{ m s}^{-1}$ ) was double that in May ( $\sim 2 \text{ m s}^{-1}$ ). Considering next the autumn time period, the SSA reconstruction reveals that the recent change associated with weakened winds in November is not unique and has occurred in the past (Figure 3c). In particular, a low-frequency oscillation in easterly wind speed is evident with an approximate 20 year period; our study period is closer to the low phase of the cycle. Interestingly, such an oscillation is not present in October (Figure 3d), where the SSA reconstruction shows a steady increase in easterly wind speeds from roughly 1985 to 2010.

What are the underlying reasons for these changes in the wind speed during the spring and fall seasons? *Brugler et al.* [2014] demonstrated that variability in the two atmospheric centers of action in the region, the Beaufort High and the Aleutian Low, have led to stronger summertime winds over the first decade of the 2000s. In particular, the Beaufort High has increased in strength [see also *Moore*, 2012], while the Aleutian Low has deepened. To shed light on the roles of both centers of action in the seasonal wind shifts documented here, we considered the atmospheric reanalysis fields from NARR. Specifically, we seek to

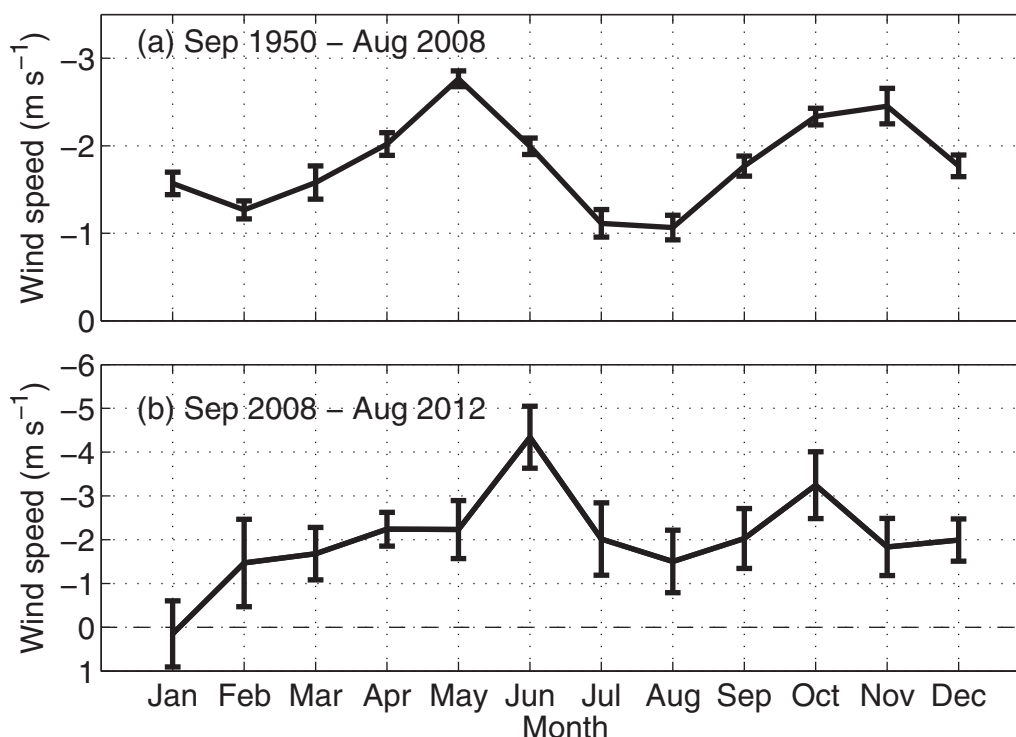


**Figure 2.** Climatological monthly mean alongcoast wind speed using data from the Pt. Barrow meteorological station for the periods (a) September 1950 to August 2008 [*Pickart et al.*, 2013a] and (b) September 2008 to August 2012, including the standard errors.

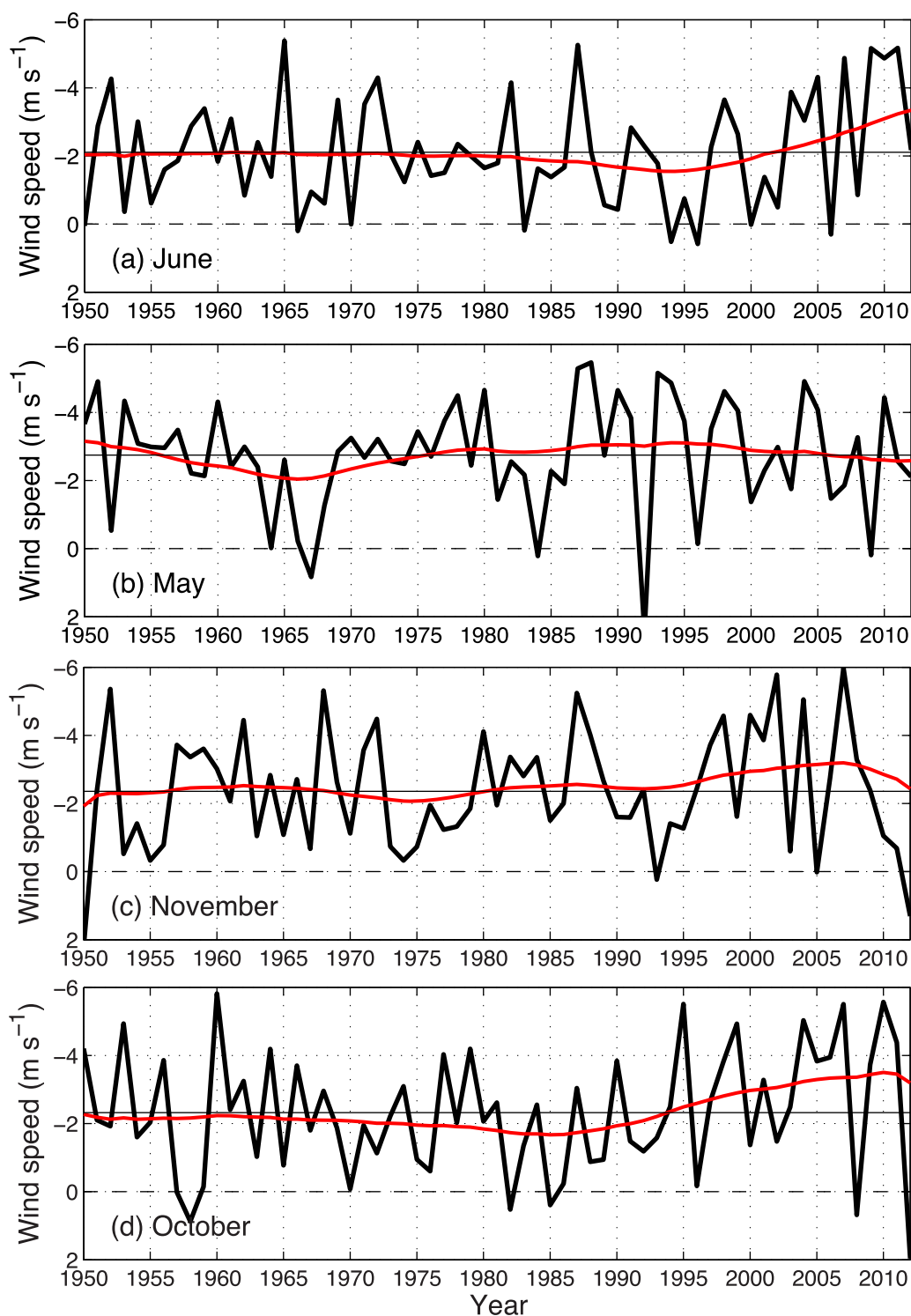


**Figure 3.** Time series of monthly averaged alongcoast wind speed at Pt. Barrow (black line), including the record-long mean (straight black line) and the low-frequency SSA reconstructions (red line, see text) (a) in June, (b) May, (c) November, and (d) October.

understand why the wind speed increased in June and decreased in October. As such, we averaged all of the SLP and wind data when the alongcoast wind speed at Pt. Barrow was greater than the long-term mean, and then did the same for those periods when the Pt. Barrow alongcoast wind speed was less than the mean. The difference between these two composites was also computed.



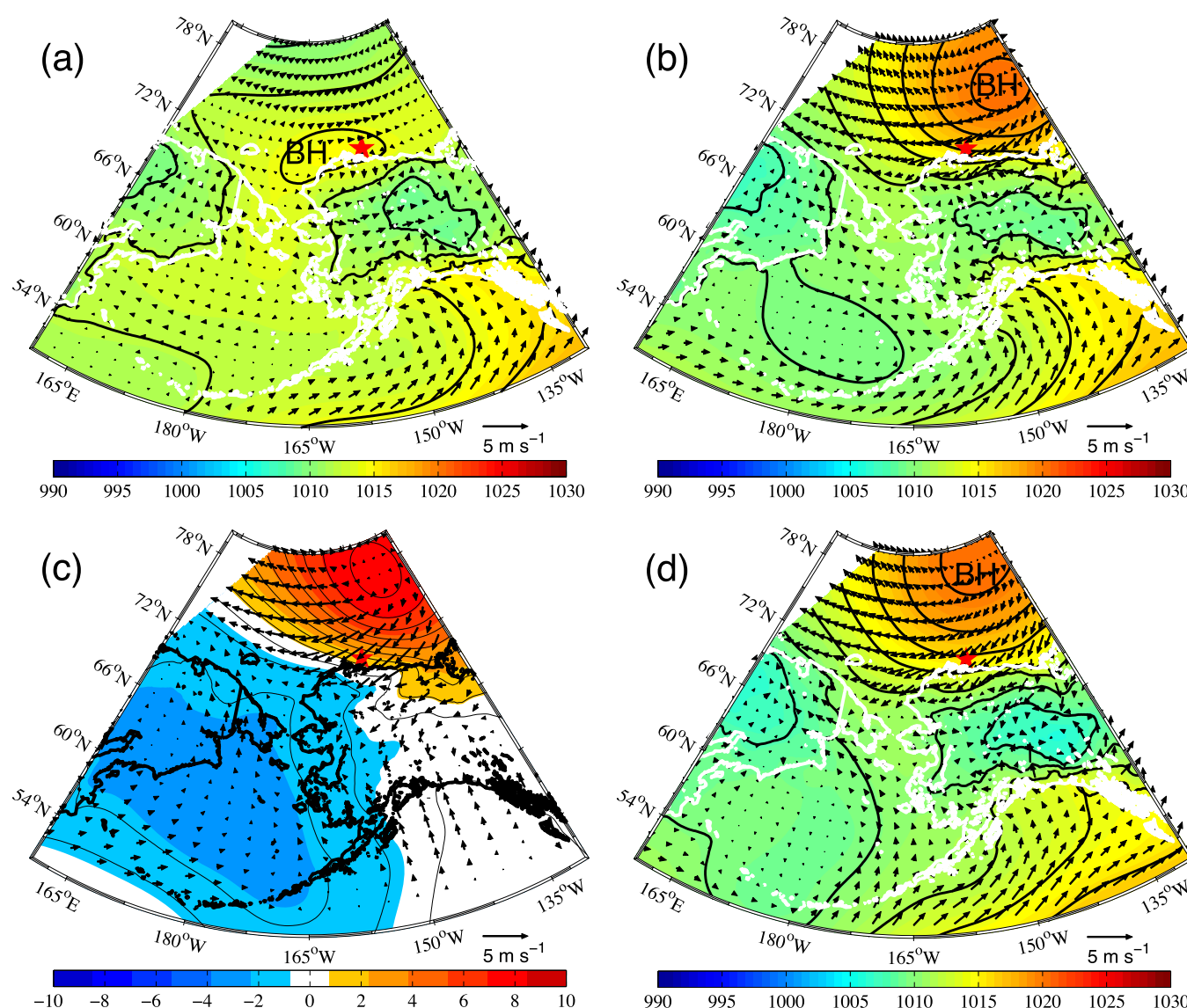


**Figure 4.** Composite SLP (contours, mb) and 10 m wind (vectors,  $\text{m s}^{-1}$ ) from NARR for the month of June (a) with wind speeds less than the long-term mean, and (b) with wind speeds larger than the long-term mean, (c) the SLP and wind difference of these two, and (d) for the time period 2009–2012. The red star denotes the location of the AON mooring. BH = Beaufort High.

For the month of June, the periods of light winds at Pt. Barrow are associated with a weak Beaufort High situated over the western Beaufort and northern Chukchi Seas (Figure 4a, roughly 48% of the time). In contrast, strong easterly winds occur when the Beaufort High is well developed and positioned over the central Beaufort Sea (Figure 4b, roughly 52% of the time). The difference field shows enhanced easterlies in a band along the Beaufort shelf and slope (Figure 4c). Note that at this time of year, there is barely any signature of the Aleutian Low. Therefore, the change in the Beaufort High dominates the difference field. Figure 4d is the composite June SLP and 10 m wind speed for the period of our study. It is evident that this time period is reflective of the strong wind composite for the month of June (compare Figures 4b and 4d).

The analogous set of figures for the month of November shows that strong winds at Pt. Barrow occur when there is a pronounced Beaufort High along with a deep Aleutian Low in the Bering Sea (Figure 5a, roughly 50% of the time). In contrast, weak winds occur when the Aleutian Low shifts eastward into the Gulf of Alaska while the Beaufort High weakens and moves westward (known at that point as the Siberian High, Figure 5b, roughly 50% of the time). The difference field in this case is characterized by westerly wind over

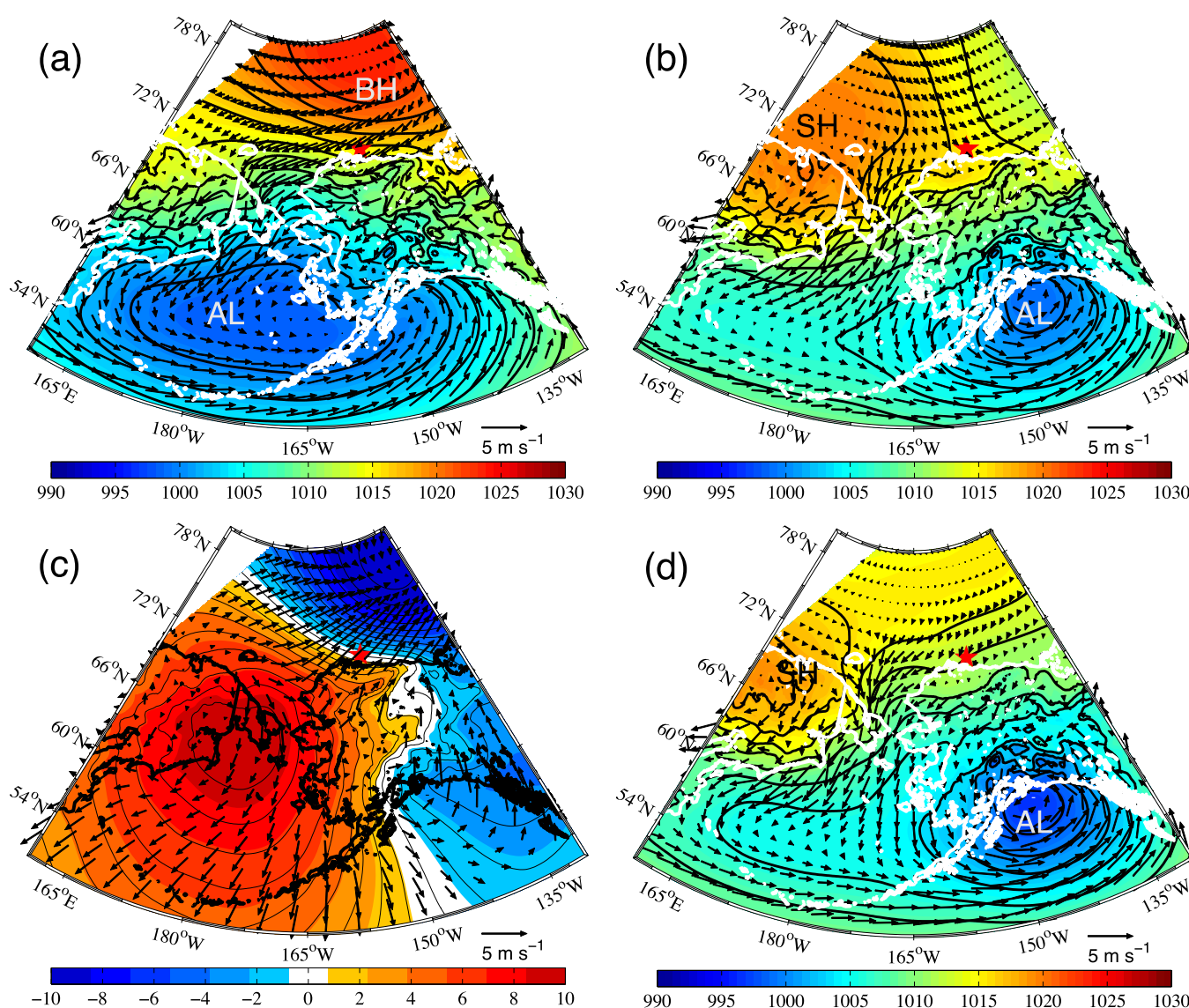


**Figure 5.** Composite SLP (contours, mb) and 10 m wind (vectors,  $\text{m s}^{-1}$ ) from NARR for the month of November (a) with wind speeds larger than the long-term mean, and (b) with wind speeds less than the long-term mean, (c) the SLP and wind difference of these two, and (d) for the time period 2008–2011. The red star denotes the location of the AON mooring. BH = Beaufort High; SH = Siberian High; AL = Aleutian Low.

the Beaufort shelf and slope (Figure 5c). Our study period is very similar in character to the weak wind composite (compare Figures 5b and 5d).

To further clarify the relative importance of the two centers of action over the course of the entire year, we performed the following procedure. First, we computed the correlation coefficient between the alongcoast wind speed at Pt. Barrow and the SLP at each point in the domain for the NARR period. This revealed a dipole structure (Figure 6a) with strong positive correlation in the northern Bering Sea and strong negative correlation in the Beaufort Sea. This is not surprising in light of the previous results, and reflects the fact that enhanced values of SLP in the Beaufort High result in stronger negative wind speeds (easterlies), while reduced SLP in the Aleutian Low also means stronger easterlies. However, this provides an objective means for choosing the two optimal locations in the domain (indicated by + symbols in Figure 6a) for assessing the importance of the two centers of action throughout the year. (We note that the pattern of correlation is nearly identical if only the summer time period is considered or only the winter time period.)

The next step was to compute a climatological monthly correlation for the NARR period between the alongcoast wind speed at Pt. Barrow and (a) the SLP at the northern location, (b) the SLP at the southern location,



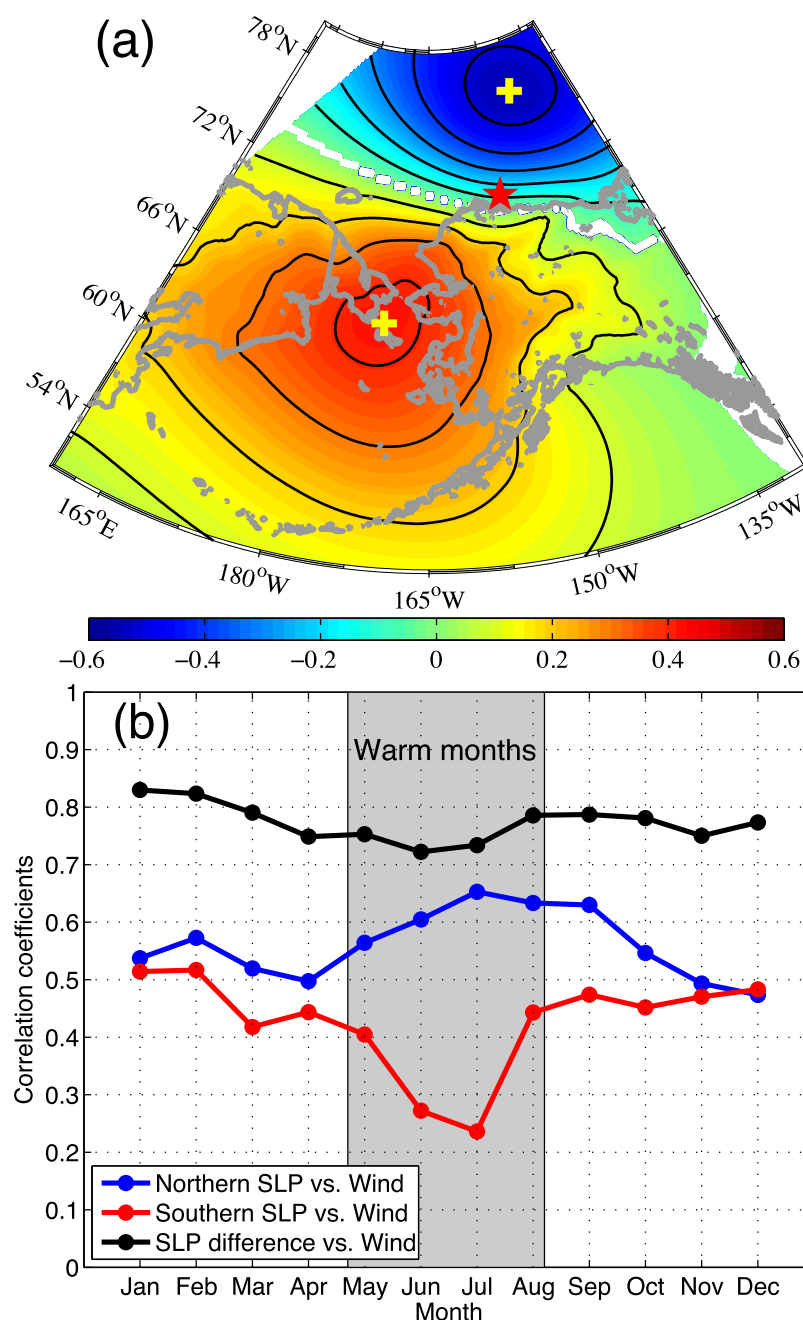


**Figure 6.** (a) Spatial distribution of correlation coefficients (the points with confidence level <95% are masked white) between time series of wind at Pt. Barrow and the time series of SLP at each point in the domain. The yellow '+'s denote the positive and negative maximum correlation coefficients, respectively, and the red star denotes the location of the AON mooring. (b) Absolute value of the monthly mean correlation coefficients (confidence level >95%) for (a) the SLP at the northern + symbol versus wind (blue line), the SLP at the southern + symbol versus wind (red line), and the SLP difference at these two locations versus wind (black line).

and (c) the difference in SLP ( $\Delta$ SLP) between the northern and southern locations. The resulting curves are taken to reflect the relative importance of each center of action alone versus the two of them working together to give rise to easterly winds in the Alaskan Beaufort Sea. The calculation was carried out by appending all of the months of January together and computing the correlation, then doing the same for each month of the year.

The three correlation coefficient curves are displayed in Figure 6b (where the absolute value is shown). The first thing to note is that the highest correlation occurs for the  $\Delta$ SLP between the two sites (black curve)

and that this value is quite high (average correlation of  $R = 0.77$  for the year). This indicates that the difference in SLP between the Beaufort High and Aleutian Low is the primary driver of easterly winds along the Beaufort slope and is also a good metric for these winds. Note, however, that the correlation is reduced during the late spring and summer. Our calculation demonstrates that this drop in correlation is due to less influence from the Aleutian Low (i.e., lower correlation of the red curve in Figure 6b), which is weakened or nearly absent during this time of year [e.g., *Favorite et al.*, 1976]. Notably, during these warm months the Beaufort High plays a more important role (higher correlation of the blue curve in Figure 6b), and in July there is in fact little difference in correlation for the  $\Delta$ SLP curve versus the northern SLP curve. This is in line with the above result showing that the behavior of the Beaufort High is main reason behind the springtime shift in easterly winds during our study period, while both centers of action play a role in the observed autumn shift.

## 4. Physical Attributes of the Beaufort Shelfbreak Jet

### 4.1. Water Masses

As presented by *Nikolopoulos et al.* [2009], the Beaufort shelfbreak jet advects predominantly Pacific water, although, in the mean, a small amount of Atlantic water (AW) is transported eastward at depth (Figure 7). This eastward transport is due to the common occurrence of upwelling [see *Pickart et al.*, 2011] (we note that the AW boundary current proper resides offshore and downslope of the Beaufort shelfbreak jet). Following *Nikolopoulos et al.* [2009], we take the potential density boundary between the Pacific and Atlantic water to be  $27.06 \text{ kg m}^{-3}$  (Figure 7). The mooring whose data are used in this study is located in the center of the shelfbreak jet, and, as such, does not measure the AW except during anomalous conditions such as upwelling (investigated below in section 4.5). Using all 4 years of mooring data, we have constructed a histogram in temperature-salinity ( $T$ - $S$ ) space showing the occurrence of the different water masses throughout water column (Figure 8a). The bounding values of temperature and salinity that define the water mass types are indicated in the figure, although the reader should realize that these boundaries are imprecise (e.g., they can change slightly from year to year [*Pisareva et al.*, 2015]). In addition to the Pacific water and AW, the mooring measured meltwater during parts of the year. One sees that the two Pacific winter waters are the most commonly measured water masses in the shelfbreak jet, especially the RWW. Regarding summer waters, the BSW is more common than the ACW, which is not surprising because some of the BSW is formed locally on the Chukchi shelf through atmospheric heating of the winter water [*Gong and Pickart*, 2015], in addition to that entering through Bering Strait. The histogram also reveals a significant presence of AW at the mooring site, which, as noted above, is due predominantly to upwelling.

Based on these water mass definitions, we have calculated the climatological monthly percentage of each water mass for the CMP measurement depth range (Figure 8b). For the first 6 months of the year the winter water dominates. It has been shown by *Nikolopoulos et al.* [2009] that during the spring, the shelfbreak jet advects these waters as a bottom-intensified current. *Spall et al.* [2008] demonstrated that this configuration of the current is baroclinically unstable which leads to eddy formation and offshore flux of cold water into the basin. While the percentage of RWW is always greater than WW, the largest percentage of the coldest, newly ventilated water occurs from January to March. After June there is a significant presence of Pacific summer water, and, during the months of July and August, BSW accounts for more than a third of the water in the shelfbreak jet. The ACW, on the other hand, peaks in September and only accounts for roughly 15% of the water. During the fall, the presence of winter water again increases, although in October there are still significant amounts of both types of summer water.

Notably, the largest percentages of AW occur in the months of May and November. Since this water mass has been observed on the shelf during upwelling events [*Pickart*, 2004; *Pickart et al.*, 2009], it suggests that such upwelling of AW is most prevalent during those 2 months, which in turn would imply that the easterly winds should be strongest then. This is at odds with the results presented above indicating that during our period of study, the months of June and October have the strongest easterlies. Some of this apparent discrepancy can be explained as follows. Close inspection reveals that the May peak in AW is dominated by the monthly value in 2010, during which the easterly winds were almost twice as strong as the other months of May (not shown). During the other 3 years the percentage of AW in May was comparable to the neighboring months. This is consistent with the fact that the peak in May is not statistically significant

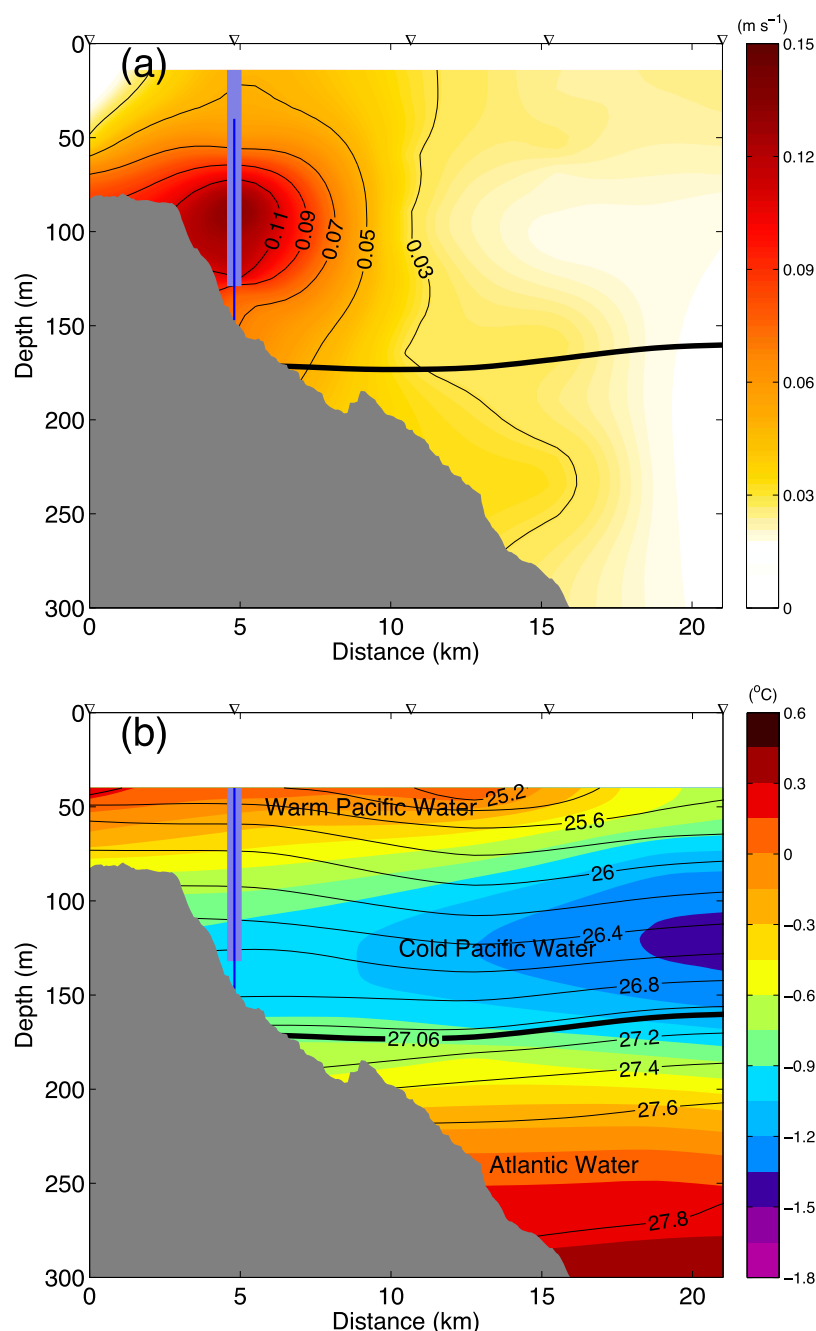


**Figure 7.** Vertical sections of (a) mean alongstream velocity ( $\text{m s}^{-1}$ ) and (b) mean potential temperature ( $^{\circ}\text{C}$ , color) overlaid by mean potential density ( $\text{kg m}^{-3}$ , contours) for the period of August 2002 to September 2004. The blue lines in Figures 7a and 7b represent the location of the AON mooring. The vertical range of the ADCP measurements is highlighted bold in Figure 7a and the vertical range of the CMP measurements is highlighted bold in Figure 7b. The thick black line is the 27.06  $\text{kg m}^{-3}$  isopycnal, which is the mean boundary between the Atlantic water and Pacific water, from *Nikolopoulos et al.* [2009].

( $P < 0.05$ ). The fall peak in AW, however, is statistically significant. At this point we have no explanation for why more AW is present in November versus October. One factor to consider is that upwelling is not only forced by local winds; it has been argued that eastward propagating shelf waves can result in upwelling along the Canadian Beaufort slope [*Carmack and Kulikov, 1998*], possibly from remote storms. Sorting this out will require additional investigation, including consideration of a larger geographical domain (which is outside the scope of this study).

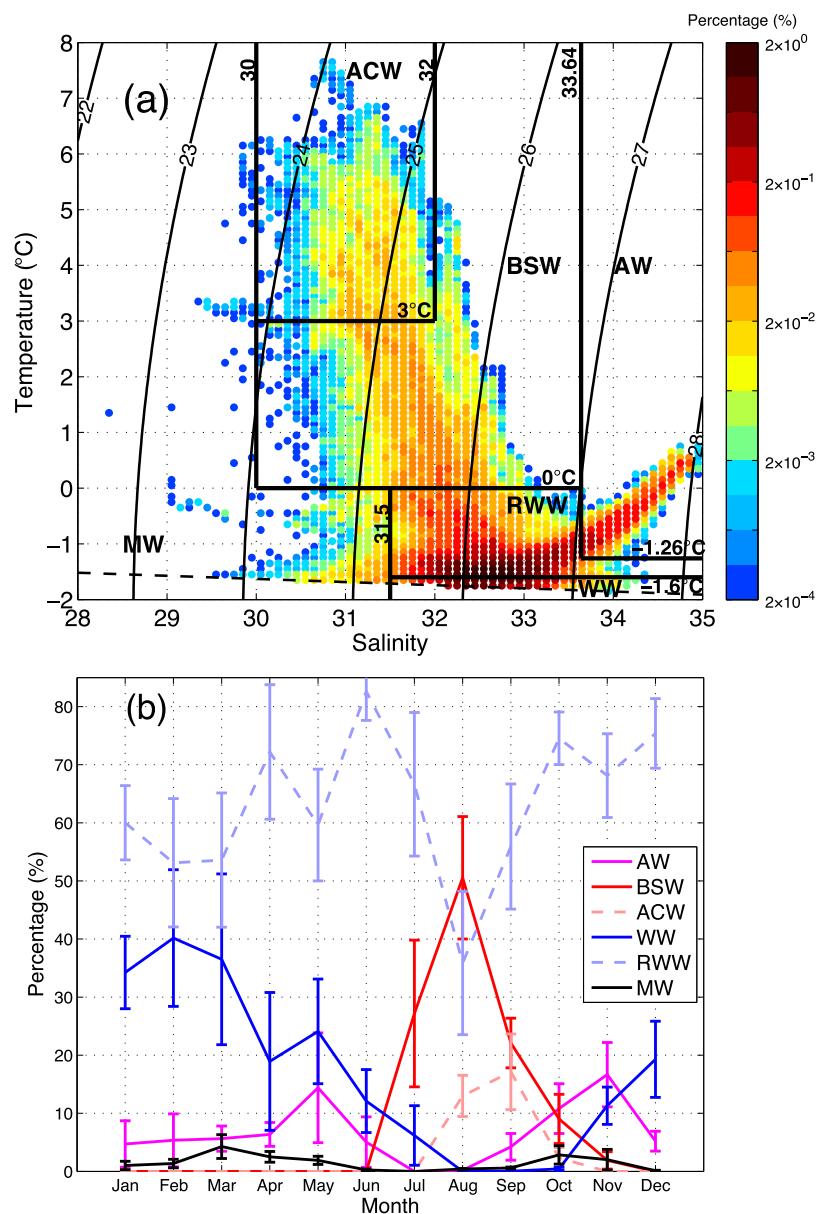


**Figure 8.** (a) Percent occurrence of T/S values using the AON CMP data for the period September 2008 to August 2012. The different water masses are marked as follows (see text): ACW = Alaskan coastal water, BSW = Bering summer water, WW = newly ventilated winter water, RWW = remnant winter water, AW = Atlantic water, and MW = melt water. (b) Climatological monthly percentages of the water masses throughout water column.

#### 4.2. Alongstream Transport

Following the method of Brugler *et al.* [2014] for computing the volume transport of the Beaufort shelfbreak jet from a single mooring, we calculated the alongstream ( $125^\circ\text{T}$ ) transport for the period September 2008 to August 2012. In line with the results of Brugler *et al.* [2014], we find that most of the transport occurs during the summer months (Figure 9, solid line). However, the maximum summer transport calculated here ( $\sim 0.15$  Sv) is less than that reported by Brugler *et al.* [2014] ( $\sim 0.25$  Sv). Furthermore, in the shoulder months of the summer (June and September) the transport in Figure 9 is negligible, yet Brugler *et al.*'s [2014] seasonal transport curve has significant eastward volume flux in these months. The reason for these differences is that Brugler *et al.* [2014] included the years of 2002–2004 in their calculation, during which time the summertime winds in the region were generally weaker (and even westerly in summer 2002) compared to our later study period (this is also in line with the increasing easterly wind trend shown in Spall *et al.* [2014]).

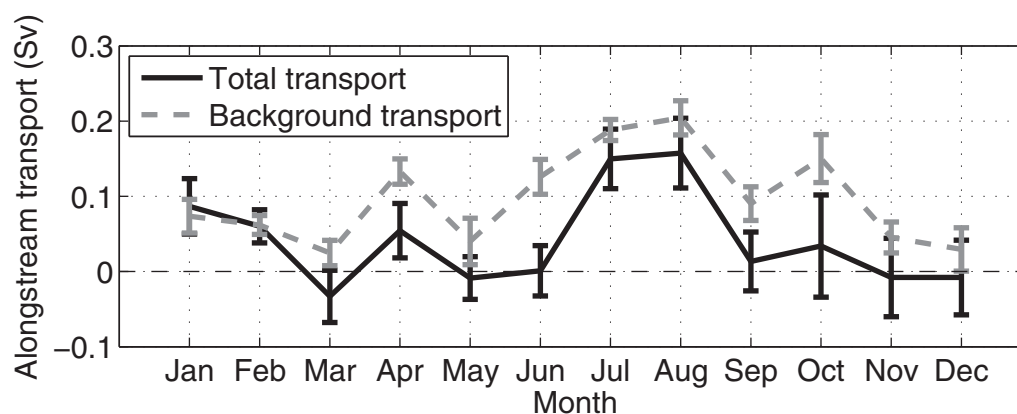


**Figure 9.** Climatological monthly mean alongstream volume transport (solid line) and background transport (dashed line) for the period September 2008 to August 2012. The standard errors are included.

The stronger easterly winds during 2008–2012 have thus resulted in diminished summer transport of the shelfbreak jet.

It is of interest to quantify the impact of the winds on the transport of the shelfbreak jet over the full annual cycle. To do this, we first computed a climatological monthly background (weak wind) transport as follows. Starting with all of the January months, we determined the time periods during which the wind speed was less than the mean minus 70% of the standard deviation. The average volume transport over these periods was then taken as the climatological monthly background value for January. The same was done for each month. We note that the 70% criterion translates on average to a wind threshold of  $3.6 \text{ m s}^{-1}$ . This is consistent with the results of Schulze and Pickart [2012] who noted that upwelling commenced for easterly wind speeds exceeding  $4 \text{ m s}^{-1}$ . Based on such a definition, the shelfbreak jet was wind-forced 72% of the time over the 4 year period. The resulting climatological monthly mean background transport is plotted in Figure 9 (dashed line). In contrast to the full transport, the background transport is to the east during every month of the year. While the seasonal variation is similar for the two curves, the background transport is generally larger—in the month of June it is greater by 0.18 Sv. Note, however, that for the month of January the background transport is less than the full transport. This is because the winds during that month tend to be out of the west (Figure 2b) which enhances the eastward transport of the shelfbreak jet.

To compute the climatological monthly mean wind-driven transport, we subtracted the monthly mean background value from the hourly time series of full transport (i.e., the background value was the same throughout each January, February, etc., over the 4 year record). This time series was then averaged climatologically for each month, and is shown in Figure 10 (black curve). Not surprisingly, the wind-driven transport is quite similar in character to the seasonal wind record (Figure 2b). In particular, the wind-driven transport is largest in the months of June and October, exceeding 0.1 Sv in both cases. This begs the question: Can we accurately predict the wind-driven transport of the shelfbreak jet using the Pt. Barrow wind record alone? To answer this, we regressed the 4 year record of wind-driven transport against the alongcoast wind speed and used the linear fit to create a monthly mean prediction (blue curve in Figure 10). While the overall agreement is good, the predicted transport does not reproduce the magnitude of the fall peak in wind-driven transport. We suspect that this discrepancy is due to the presence of pack ice, which is investigated as follows.

Both the ice concentration in this region, as well as the ice thickness, vary significantly throughout the year (Figure 11). The monthly mean ice concentration was computed from satellite data (the average value within the blue box in Figure 1), and the ice thickness was measured from the mooring (see section 2.1). The two curves are similar that during late summer and early fall, there is very little ice and it is quite thin. However, during the winter and spring (January–May) the ice concentration stays nearly the same, while the thickness varies considerably. It is important to note that the climatological mean value of ice thickness is significantly different from zero for each month of the year for our study period (the confidence level is >95%); even from August through October there was measurable ice at the mooring site (mean thickness of 8 cm for the 3 months).



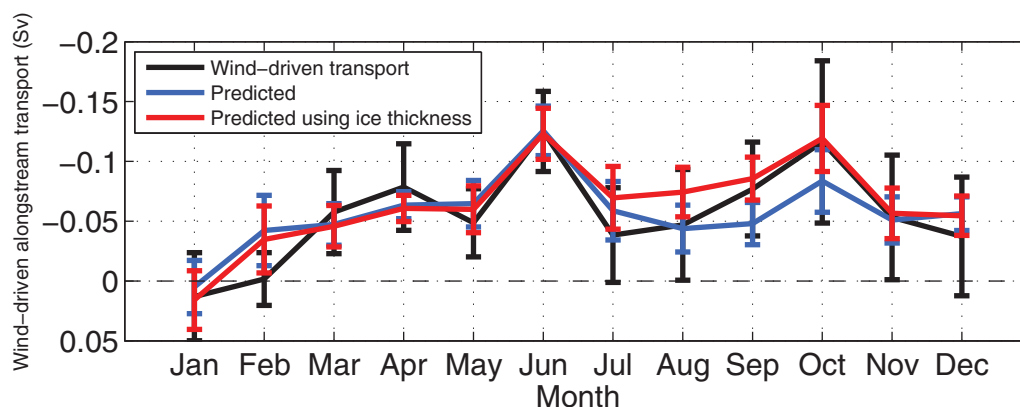


**Figure 10.** Climatological monthly mean alongstream wind-driven transport (black line), predicted wind-driven transport using a single regression (blue line), and predicted wind-driven transport using a set of regressions corresponding to ice thickness (red line, see text for details) for the period September 2008 to August 2012. The standard errors are included.

This suggests that the presence of ice could impact the relationship between the wind speed and the wind-driven transport of the jet. Indeed, this is evident when plotting the ice thickness in relation to the alongstream wind-driven transport (Figure 12a). It is seen that the range in observed transport decreases markedly for thicker ice (noting that most of the measured ice drafts are  $<6$  m). This makes sense that internal ice stresses will be more apt to absorb energy from the wind when the ice is consolidated into thick, less movable floes. With this in mind we computed a separate set of linear regressions between the wind speed and wind-driven transport for different ranges of ice thickness. In particular, we distinguished time periods based on the measured ice thickness: a 20 cm bin size for drafts less than 4 m, and 1 m interval for that thicker than 4 m (to get enough samples in each bin). Then a linear fit of wind-driven transport versus wind speed over the full 4 year period was calculated for each ice thickness range (the confidence level is  $>95\%$ ).

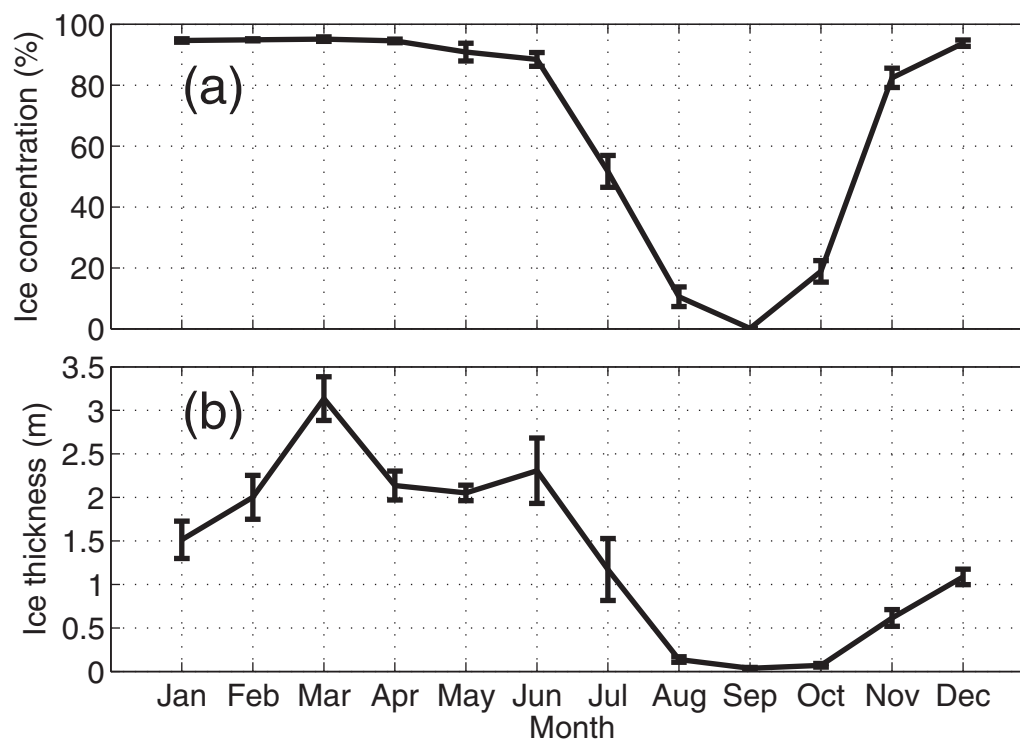


**Figure 11.** Climatological monthly mean (a) ice concentration and (b) ice thickness for the period September 2008 to August 2012. The standard errors are included.

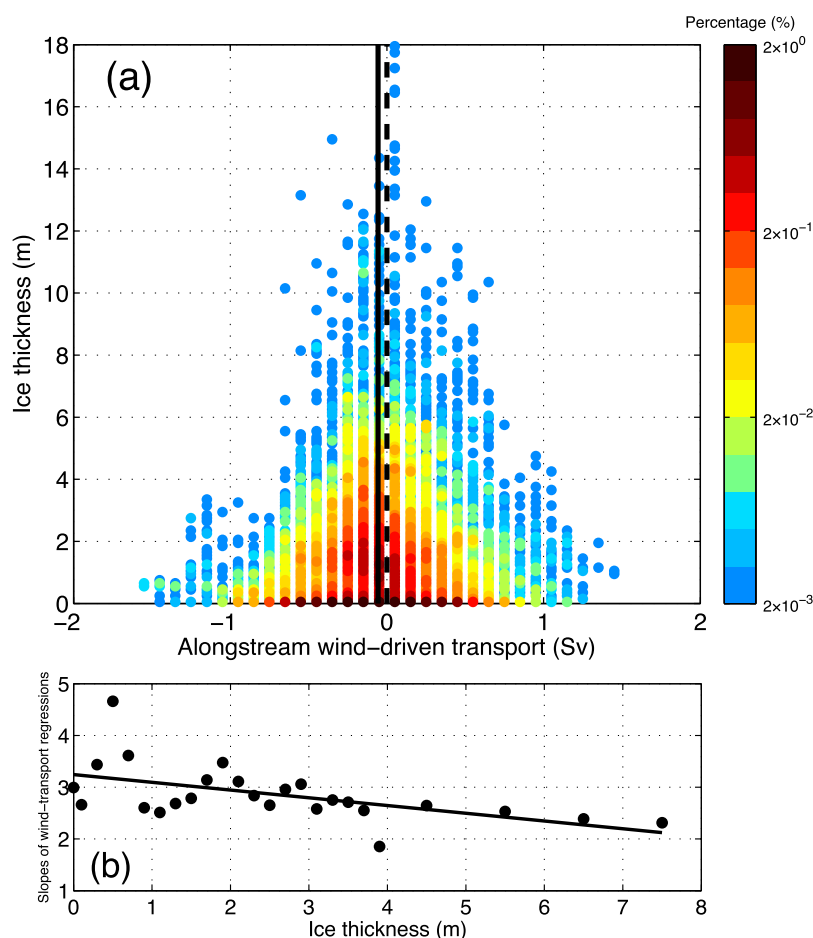


**Figure 12.** (a) Ice thickness versus alongstream wind-driven transport, colored by the percent occurrence (%). The black line represents the mean alongstream wind-driven transport. (b) Slopes ( $\times 10^{-2}$ ) of alongcoast wind speed versus alongstream wind-driven transport regressions. The line of best fit is shown.

for these regressions). The slopes of the regression lines tend toward smaller values for thicker ice (Figure 12b), implying that, in general, thicker ice is associated with less wind-driven enhancement of the shelf-break jet.

Following the analogous procedure as above, except using this new set of regressions rather than a single overall regression, we produced a second predicted monthly mean wind-driven transport curve (red curve in Figure 10) which now empirically accounts for the effect of ice. For all months of the year except for mid-summer to mid-fall, the ice-adjusted predicted transport is smaller than the prediction using wind alone. However, the differences are minor, implying that for the most part, the pack-ice is mobile even when it is thick. Notably, during July to October—when the ice is thin—the ice-adjusted value exceeds the wind-only prediction. The reason for this is likely because, for a sparse ice cover, the ice-ocean stress enhances the wind-driven response of the ocean; to wit, *Schulze and Pickart* [2012] found that the upwelling response of the shelfbreak jet to easterly wind events was greatest for a partial ice cover, which is in line with the numerical model results of *Martin et al.* [2014]. This is consistent with the large regression slope for the 40–60 cm ice bin in Figure 12b. These results imply that the ice concentration plays a greater role in modulating the wind-driven transport of the shelfbreak jet than the ice thickness (although we are unable to confirm this because meaningful regressions cannot be made using the less frequent satellite ice concentration data).

### 4.3. Upwelling

One of the dominant modes of variability in the Beaufort shelfbreak jet is wind-forced upwelling, which can drive significant cross-stream fluxes of heat, salt, nutrients, and carbon [*Mathis et al.*, 2012; *Pickart et al.*,

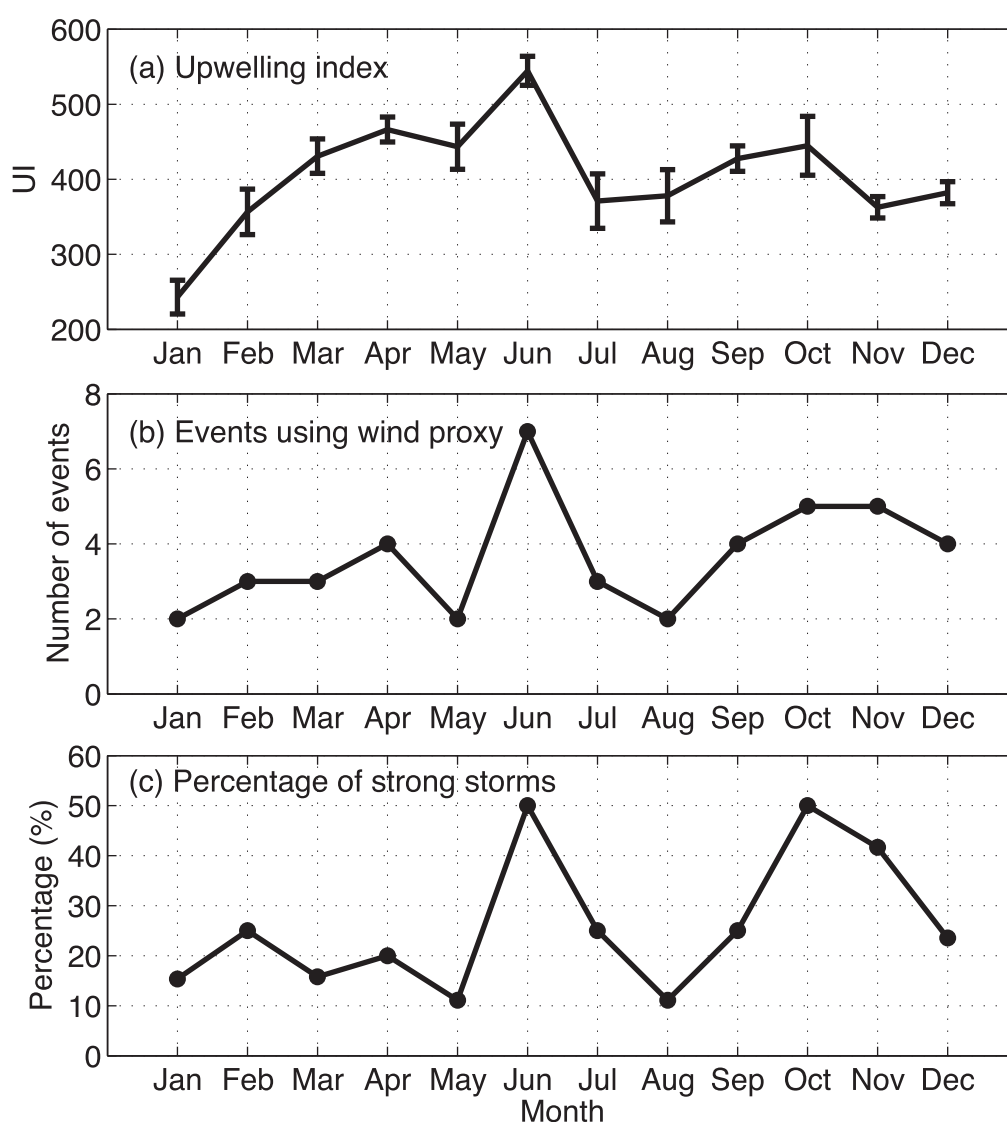


**Figure 13.** (a) Climatological monthly mean upwelling index (UI) for the period September 2008 to August 2012. The standard errors are included. (b) Monthly number of upwelling events using the wind proxy for the periods September 2008 to August 2012. (c) Monthly percentage of strong storms relative to all upwelling storms.

2013b]. In addition, zooplankton can be fluxed shoreward which can impact cetacean feeding behavior [Okkonen *et al.*, 2011]. As such, we now assess the seasonality of upwelling during our study period as deduced from the mooring data. We defined an upwelling index (UI) for each easterly wind event over the 4 year record

$$UI = \int_{t_s + t_d}^{t_e + t_d} \frac{\rho(t)}{\rho|_{t=t_s + t_d}} dt,$$

where  $\rho$  is the potential density at bottom of the mooring, and  $t_s$ ,  $t_e$  are start time and end time of each easterly wind event. On average the potential density response of the water column lagged the wind by 21 h, and this delay time  $t_d$  is taken into account in the index. Defined as such, UI reflects both the magnitude and length of the event. (We note that a small fraction of easterly wind events did not result in upwelling, and these events are not considered in the results below.)

The climatological monthly mean value of UI for the period September 2008 to August 2012 shows a similar pattern to that of the wind speed (compare Figure 13a to Figure 2b). In particular, both curves have a peak

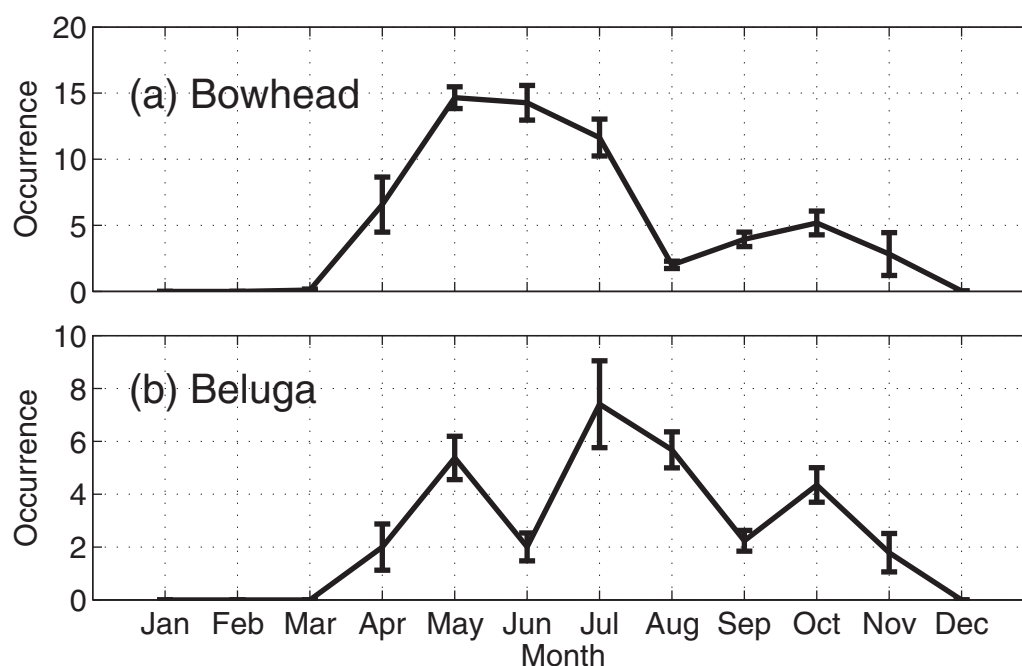


**Figure 14.** Climatological monthly mean occurrences of (a) bowhead and (b) beluga whales for the period September 2008 to August 2012. The standard errors are included.

in June and October. The only substantial difference is that even though the easterly winds are somewhat comparable in strength during the transition from winter to spring (February–April), the intensity in upwelling increases during this time. This might be due to ice inhibiting the magnitude of the oceanic response in winter, consistent with the results of *Schulze and Pickart* [2012].

The generally good agreement between UI and the wind speed motivates us to consider the wind proxy for identifying upwelling events that was employed by *Pickart et al.* [2013a]. Following those authors, we identified all of the wind events in the Pt. Barrow alongcoast easterly wind record that lasted 4 days or longer and exceeded  $10 \text{ m s}^{-1}$  at some point during the storm. (Such storms were considered by *Pickart et al.* [2013a] to be strong enough to induce upwelling.) The seasonality of these strong upwelling events defined by the proxy over our 4 year period is similar to the UI curve that a greater number of strong storms occurred in June and in the fall (compare Figures 13a and 13b). This indicates that these powerful storms are responsible for the dominant upwelling signals (i.e., the largest values of UI).

It should be noted, however, that many smaller storms not identified by the wind proxy resulted in upwelling along the Beaufort slope according to the mooring time series. In fact, the proxy missed more than 70% of the upwelling events. Over the 4 year period, the mooring data revealed that there were 181 upwelling events, while the proxy only identified 44 events (all of which were verified by the mooring as well). Figure 13c shows the monthly variation in the percentage of strong storms (i.e., those identified by the proxy) to all of the wind-driven upwelling storms (even those with a small signal). Interestingly, the percentage is highest for the months of June and October, the two months when UI was greatest (Figure 13a) and the alongcoast wind speed was greatest as well (Figure 2b). This again highlights the important role of strong storms in dictating the seasonal signal of upwelling in the shelfbreak jet.

## 5. Cetacean Occurrence in the Vicinity of the Shelfbreak Jet

Following the above analysis of the physical features of the shelfbreak jet, we computed the climatological monthly mean occurrence of the two types of cetaceans at the mooring site for our study period (Figure 14). Both beluga and bowhead whales show clear seasonal patterns indicative of eastward migration in the spring and westward migration in the fall. For the bowheads, there is a large peak in occurrence from May to July and a smaller peak in October (Figure 14a). The timing of the first peak, associated with the eastward

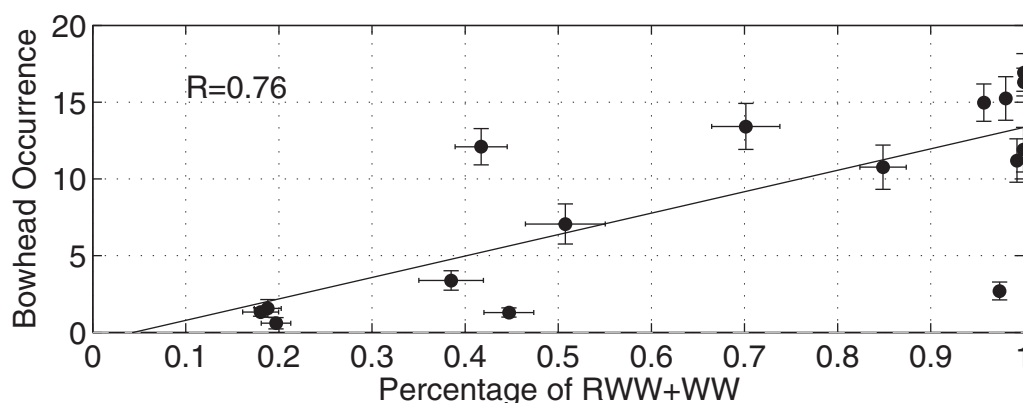


**Figure 15.** Monthly mean Bowhead occurrence (number/day) versus monthly percentage of both RWW and WW. The regression line is shown, and the standard errors are included.

migration to the Canadian Beaufort Sea, is likely dictated by the pack ice cover. Despite the fact that Arctic marine mammals are ice-adapted they require access to air in order to breathe, and by May both the ice concentration and thickness have begun to decrease at the mooring location (Figure 11). Typically, melt-back occurs in a swath along the western Beaufort shelf/slope [Steele *et al.*, 2015], which would force the whales to stay fairly close to the boundary as they head east toward their summer feeding grounds in the region of Cape Bathurst.

During the fall migration period, however, the ice edge has normally receded well into the basin, and so bowhead whales would be largely unrestricted in their movements. This seems to be the case during our study period 2008–2012, as the number of bowhead calls at the mooring site in autumn was much reduced from that in the spring, and the autumn ice edge was far offshore in each of the years. Notably, however, there is a peak in the month of October, which, as discussed above, is also associated with a peak in the percentage of strong upwelling storms and the value of UI (Figure 13). This is likely causal that the upwelled water from the basin brings high nutrient, zooplankton-rich water toward the boundary which will attract the bowheads. This is consistent with observations near Barrow Canyon where upwelling favorable conditions lead to higher occurrences of bowheads [Ashjian *et al.*, 2010; Citta *et al.*, 2015]. In terms of water masses, cold Pacific winter water generally contains the highest concentrations of nitrate [e.g., Lowry *et al.*, 2015] that will spur primary production and, in turn, secondary production. We found a significant relationship between the monthly mean occurrence of bowhead whales and the percentage of WW+RWW ( $R = 0.76$  with confidence level  $>95\%$ , Figure 15).

The peaks in beluga occurrence in May and July represent differences in the migratory timing in spring/summer of the two different populations of this species, the Beaufort Sea population (April–May) and Eastern Chukchi Sea population (July–August). The peak in October is presumed to represent the westward migration of Eastern Chukchi Sea whales [Stafford *et al.*, 2016b]. As was the case for the bowheads, the enhanced upwelling in the month of October is likely to bring prey-rich waters toward the boundary, in this case Arctic cod which feed on the zooplankton. Previous data from the region of Barrow Canyon have shown that beluga whale vocalizations increase there in early fall as the Beaufort shelfbreak jet—which is the eastward extension of the ACC at this time of year—sets up a front that is thought to concentrate the prey [Stafford *et al.*, 2013]. When the ACC weakens, belugas are thought to spend more time at depth near the boundary between cold Pacific water and relatively warm Atlantic water (Figure 8b) [Stafford *et al.*, 2016a]. Determining if the physical drivers associated with the boundary current influence shorter timescale variation in whale occurrence will require a more detailed examination of the data.

## 6. Conclusions

In this study we have quantified the seasonal variations of the Beaufort shelfbreak jet and Arctic cetacean occurrence for the time period 2008–2012 using data from a pair of moorings near 152°W, approximately



150 km east of Pt. Barrow, AK, together with atmospheric reanalysis fields and satellite ice concentration data. The atmospheric forcing during this 4 year period differs from the long-term climatological conditions in that the springtime peak in easterly winds shifted from May to June, and the autumn peak was confined to the month of October (instead of extending into November).

In line with the previous studies, we found that the two atmospheric centers of action, the Beaufort High and Aleutian Low, predominantly control the wind conditions in our study region. By constructing composite sea level pressure and wind fields we determined that an intensified Beaufort High caused the enhanced winds in June, while the relative locations and magnitudes of both the Beaufort High and Aleutian Low played key roles in the change in the autumn wind peak.

The Beaufort shelfbreak jet advects predominantly Pacific water with a clear seasonal progression. The two summer waters, Bering summer water and Alaskan coastal water, are most prevalent during August and September, respectively, although the percentage of Alaskan coastal water is much less. The newly ventilated Pacific winter water, which is fairly close to the freezing point, is most common from January to March, while the remnant winter water is present in significant amounts throughout the year with a minimum in August.

In line with the results of *Brugler et al.* [2014], we found that most of the eastward volume transport of the current occurs in summer. We decomposed the annual variation in transport into a background component and a wind-driven component. The background value was computed by considering those times when the alongcoast wind speed is less than the monthly mean minus 70% of the standard deviation, and the wind-driven value was taken as the difference between the background transport and total transport. The wind-driven transport is largest in the months of June and October, consistent with the wind peaks during those months. However, using the alongcoast wind speed alone to predict the wind-driven transport underestimates the fall peak. Using the ice thickness data we argue that this discrepancy is due to the effects of the freely moving pack-ice during this time of year. This is consistent with earlier studies demonstrating that the ice-ocean stress enhances the wind-driven response for a partial ice cover [*Pickart et al.*, 2013b; *Martin et al.*, 2014]. We defined an upwelling index that takes into account the density of the upwelled water as well as the length of time that it resides near the shelfbreak. Not surprisingly, the seasonality of this index reveals that upwelling is most intense during the months of June and October when the easterly winds are strongest. Further analysis showed that this was associated with generally fewer, long-lasting storms versus a larger number of shorter storms indicative of other months.

The seasonality of bowhead and beluga whales in the Beaufort shelfbreak jet was investigated by computing climatological monthly means of the number of vocal occurrences of each species and comparing this to the physical characteristics of the current and overall environmental conditions. The passive acoustic data showed evidence of the eastward spring migration and westward fall migration of the two cetaceans. The former is dictated largely by the ice cover which recedes along the southern boundary of the Beaufort Sea, keeping the whales close to the mooring site. In the fall there is a peak in call occurrence of both the bowheads and belugas, which coincides with the peak in the intensity of the upwelling. Such nutrient-rich upwelled water has high concentrations of zooplankton—and likely Arctic cod that feed on the zooplankton—which could attract the cetaceans. As the ice continues to retreat in the Beaufort Sea [*Laidre et al.*, 2015], and upwelling becomes more common [*Pickart et al.*, 2013a], our results suggest that the seasonality of the bowheads and belugas will be altered accordingly. By understanding the physical drivers of a region, it may be possible to predict how climatological changes in the environment will affect the phenology of Arctic cetaceans.

#### Acknowledgments

The authors would like to thank the officers and crew of the USCGC Healy, along with John Kemp and Jim Ryder, for the successful mooring operations. Catherine Berchok of the National Marine Fisheries Service turned around the acoustic recorder mooring annually. Carolina Nobre provided programming assistance during the analysis of the data. Support for the most recent deployments of the shelfbreak moorings was provided by grants ARC-0856244 and ARC-855828 from the Office of Polar Programs of the National Science Foundation. P.L. acknowledges the financial support of the China Scholarship Council. The moored time series and passive acoustic data used to determine cetacean occurrence are available from: [https://www.aoncadis.org/project/collaborative\\_research\\_and\\_interdisciplinary\\_monitoring\\_mooring\\_in\\_the\\_western\\_arctic\\_boundary\\_current\\_climatic\\_forcing\\_and\\_ecosystem\\_response.html](https://www.aoncadis.org/project/collaborative_research_and_interdisciplinary_monitoring_mooring_in_the_western_arctic_boundary_current_climatic_forcing_and_ecosystem_response.html).

#### References

- Aagaard, K. (1984), The Beaufort Undercurrent, in *The Alaskan Beaufort Sea*, edited by P. W. Barnes, D. M. Schell, and E. Reimnitz, pp. 47–71, Academic, San Diego, Calif.
- Aagaard, K., and A. T. Roach (1990), Arctic ocean-shelf exchange: Measurements in Barrow Canyon, *J. Geophys. Res.*, 95(C10), 18,163–18,175, doi:10.1029/JC095iC10p18163.
- Aagaard, K., T. Weingartner, S. L. Danielson, R. A. Woodgate, G. C. Johnson, and T. E. Whitledge (2006), Some controls on flow and salinity in Bering Strait, *Geophys. Res. Lett.*, 33, L19602, doi:10.1029/2006GL026612.
- Ashjian, C. J., et al. (2010), Climate variability, oceanography, bowhead whale distribution, and inupiat subsistence whaling near Barrow, Alaska, *Arctic*, 63, 179–194.
- Brugler, E. T., R. S. Pickart, G. W. K. Moore, S. Roberts, T. J. Weingartner, and H. Statscewich (2014), Seasonal to interannual variability of the Pacific water boundary current in the Beaufort Sea, *Prog. Oceanogr.*, 127, 1–20, doi:10.1016/j.pocean.2014.05.002.

- Carmack, E. C., and E. A. Kulikov (1998), Wind-forced upwelling and internal Kelvin wave generation in Mackenzie Canyon, Beaufort Sea, *J. Geophys. Res.*, *103*(C9), 18,447–18,458, doi:10.1029/98JC00113.
- Citta, J. J., et al. (2015), Ecological characteristics of core-use areas used by Bering–Chukchi–Beaufort (BCB) bowhead whales, 2006–2012, *Prog. Oceanogr.*, *136*, 201–222.
- Favorite, F., A. J. Dodimead, and K. Nasu (1976), Oceanography of the subarctic Pacific region, 1962–1972, *Bull. Int. North Pac. Comm.*, *33*, 1–187.
- Fratantoni, P. S., S. Zimmermann, R. S. Pickart, and M. Swartz (2006), Western Arctic Shelf-basin Interaction Experiment: Processing and calibration of moored profiler data from the Beaufort shelf-edge mooring array, *Tech. Rep. WHOI-2006-15*, 34 pp., Woods Hole Oceanogr. Inst., Woods Hole, Mass.
- Frost, K. J., and L. F. Lowry (1984), *Trophic Relationships of Vertebrate Consumers in the Alaskan Beaufort Sea*, edited by P. W. Barnes, D. M. Schell, and E. Reimnitz, pp. 381–401, Academic, Orlando, Fla.
- George, J. C., M. L. Druckenmiller, K. L. Laidre, R. Suydam, and B. Person (2015), Bowhead whale body condition and links to summer sea ice and upwelling in the Beaufort Sea, *Prog. Oceanogr.*, *136*, 250–262.
- Ghil, M., et al. (2002), Advanced spectral methods for climatic time series, *Rev. Geophys.*, *40*(1), 1003, doi:10.1029/2000RG000092.
- Gong, D., and R. S. Pickart (2015), Summertime circulation in the Eastern Chukchi Sea, *Deep Sea Res., Part II*, *105*, 53–73.
- Häkkinen, S. (1986), Coupled ice-ocean dynamics in the marginal ice zones: Upwelling/downwelling and eddy generation, *J. Geophys. Res.*, *91*(C1), 819–832, doi:10.1029/JC0911C01p00819.
- Hassani, H. (2007), Singular spectrum analysis: Methodology and comparison, *J. Data Sci.*, *5*, 239–257.
- Hauser, D., K. L. Laidre, R. S. Suydam, and P. R. Richard (2014), Population-specific home ranges and migration timing of Pacific Arctic beluga whales (*Delphinapterus leucas*), *Polar Biol.*, *37*, 1171–1183.
- Hufford, G. L. (1974), On apparent upwelling in the southern Beaufort Sea, *J. Geophys. Res.*, *79*(9), 1305–1306, doi:10.1029/JC079i009p01305.
- Itoh, M., et al. (2015), Water properties, heat and volume fluxes of Pacific water in Barrow Canyon during summer 2010, *Deep Sea Res., Part I*, *102*, 43–54.
- Karcher, M., F. Kauker, R. Gerdes, E. Hunke, and J. Zhang (2007), On the dynamics of Atlantic Water circulation in the Arctic Ocean, *J. Geophys. Res.*, *112*, C04502, doi:10.1029/2006JC003630.
- Laidre, K. L., et al. (2015), Arctic marine mammal population status, sea ice habitat loss, and conservation recommendations for the 21st century, *Conserv. Biol.*, *29*, 724–737.
- Loseto, L. L., G. A. Stern, T. L. Connelly, D. Deibel, B. Gemmill, A. Prokopenko, L. Fortier, and S. H. Ferguson (2009), Summer diet of beluga whales inferred by fatty acid analysis of the eastern Beaufort Sea food web, *J. Exp. Mar. Biol. Ecol.*, *374*, 12–18.
- Lowry, K. E., et al. (2015), The influence of winter water on phytoplankton blooms in the Chukchi Sea, *Deep Sea Res., Part II*, *118*, 53–72.
- Martin, T., M. Steele, and J. Zhang (2014), Seasonality and long-term trend of Arctic Ocean surface stress in a model, *J. Geophys. Res. Oceans*, *119*, 1723–1738, doi:10.1002/2013JC009425.
- Mathis, J. T., et al. (2012), Storm-induced upwelling of high pCO<sub>2</sub> waters onto the continental shelf of the western Arctic Ocean and implications for carbonate mineral saturation states, *Geophys. Res. Lett.*, *39*, L07606, doi:10.1029/2012GL051574.
- Mesinger, F., et al. (2006), North American regional reanalysis, *Bull. Am. Meteorol. Soc.*, *87*, 343–360.
- Moore, G. W. K. (2012), Decadal variability and a recent amplification of the summer Beaufort Sea High, *Geophys. Res. Lett.*, *39*, L10807, doi:10.1029/2012GL051570.
- Moore, S. E. (2000), Variability of Cetacean distribution and habitat selection in the Alaskan Arctic, autumn 1982–91, *Arctic*, *53*, 448–460.
- Nikolopoulos, A., R. S. Pickart, P. S. Fratantoni, K. Shimada, D. J. Torres, and E. P. Jones (2009), The western Arctic boundary current at 152°W: Structure, variability, and transport, *Deep Sea Res., Part II*, *56*, 1164–1181, doi:10.1016/j.dsr2.2008.10.014.
- Okkonen, S. R., C. Ashjian, R. Campbell, J. Clarke, S. E. Moore, and K. Taylor (2011), Satellite observations of circulation features associated with a bowhead whale feeding “hotspot” near Barrow, Alaska, *Remote Sens. Environ.*, *115*, 2168–2174.
- Paquette, R. G., and R. H. Bourke (1979), Temperature fine structure near the Sea-ice margin of the Chukchi Sea, *J. Geophys. Res.*, *84*(C3), 1155–1164, doi:10.1029/JC084iC03p01155.
- Pickart, R. S. (2004), Shelfbreak circulation in the Alaskan Beaufort Sea: Mean structure and variability, *J. Geophys. Res.*, *109*, C04024, doi:10.1029/2003JC001912.
- Pickart, R. S., G. W. K. Moore, D. J. Torres, P. S. Fratantoni, R. A. Goldsmith, and J. Yang (2009), Upwelling on the continental slope of the Alaskan Beaufort Sea: Storms, ice, and oceanographic response, *J. Geophys. Res.*, *114*, C00A13, doi:10.1029/2208JC005009.
- Pickart, R. S., M. A. Spall, G. W. K. Moore, T. J. Weingartner, R. A. Woodgate, K. Aagaard, and K. Shimada (2011), Upwelling in the Alaskan Beaufort Sea: Atmospheric forcing and local versus non-local response, *Prog. Oceanogr.*, *88*, 78–100, doi:10.1016/j.pocean.2010.11.005.
- Pickart, R. S., L. M. Schulze, G. W. K. Moore, M. A. Charette, K. Arrigo, G. van Dijken, and S. Danielson (2013a), Long-term trends of upwelling and impacts on primary productivity in the Alaskan Beaufort Sea, *Deep Sea Res., Part I*, *79*, 106–121.
- Pickart, R. S., M. A. Spall, and J. T. Mathis (2013b), Dynamics of upwelling in the Alaskan Beaufort Sea and associated shelf-basin fluxes, *Deep Sea Res., Part I*, *76*, 35–51.
- Pickart, R. S., G. W. K. Moore, C. Mao, F. Bahr, C. Nobre, T. J. Weingartner (2016), Circulation of winter water on the Chukchi Shelf in early summer, *Deep Sea Res., Part II*, *130*, 56–75.
- Pisareva, M. N., R. S. Pickart, M. Spall, C. Nobre, D. J. Torres, G. W. K. Moore, and T. E. Whiteledge (2015), Flow of Pacific water in the western Chukchi Sea: Results from the 2009 RUSALCA expedition, *Deep Sea Res., Part I*, *105*, 53–73.
- Quakenbush, L. T., R. S. Suydam, A. L. Brown, L. F. Lowry, K. J. Frost, and B. A. Mahoney (2015), Diet of beluga whales, *Delphinapterus leucas*, in Alaska from stomach contents, March–November, *Mar. Fish. Rev.*, *77*, 70–84.
- Reynolds, R. W., T. M. Smith, C. Liu, D. B. Chelton, K. S. Casey, and M. G. Schlax (2007), Daily high-resolution-blended analyses for sea surface temperature, *J. Clim.*, *20*(22), 5473–5496, doi:10.1175/2007JCLI1824.1.
- Røed, L. P., and J. J. O’Brien (1983), A coupled ice-ocean model of upwelling in the marginal ice zone, *J. Geophys. Res.*, *88*(C5), 2863–2872, doi:10.1029/JC088iC05p02863.
- Rudels, B., E. P. Jones, U. Schauer, and P. Eriksson (2004), Atlantic sources of the Arctic Ocean surface and halocline waters, *Polar Res.*, *23*(2), 181–208.
- Schulze, L. M., and R. S. Pickart (2012), Seasonal variation of upwelling in the Alaskan Beaufort Sea: Impact of sea ice cover, *J. Geophys. Res.*, *117*, C06022, doi:10.1029/2012JC007985.
- Shimada, K., Carmack, E. C., Hatakeyama, K. and Takizawa, T. (2001), Varieties of shallow temperature maximum waters in the Western Canadian Basin of the Arctic Ocean, *Geophys. Res. Lett.*, *28*, 3441–3444, doi:10.1029/2001GL013168.
- Shimada, K., T. Kamoshida, M. Itoh, S. Nishino, E. Carmack, F. McLaughlin, S. Zimmermann, and A. Proshutinsky (2006), Pacific Ocean inflow: Influence on catastrophic reduction of sea ice cover in the Arctic Ocean, *Geophys. Res. Lett.*, *33*, L08605, doi:10.1029/2005GL025624.

- Spall, M. A., R. S. Pickart, P. S. Fratantoni, and A. J. Plueddemann (2008), Western arctic shelf break eddies: Formation and transport, *J. Phys. Oceanogr.*, **38**, 1644–1668, doi:10.1175/2007JPO3829.1.
- Spall, M. A., R. S. Pickart, E. T. Brugler, G. W. K. Moore, L. Thomas, and K. R. Arrigo (2014), Role of shelfbreak upwelling in the formation of a massive under-ice bloom in the Chukchi Sea, *Deep Sea Res., Part I*, **105**, 17–29.
- Stafford, K. M., S. R. Okkonen, and J. T. Clarke (2013), Correlation of a strong Alaska Coastal Current with the presence of beluga whales *Delphinapterus leucas* near Barrow, Alaska, *Mar. Ecol. Prog. Ser.*, **474**, 287–297.
- Stafford, K. M., J. J. Citta, S. R. Okkonen, and R. S. Suydam (2016a), Wind-dependent beluga whale dive behavior in Barrow Canyon, Alaska, *Deep Sea Res., Part I*, 1–19, doi:10.1016/j.dsr.2016.10.006.
- Stafford, K. M., et al. (2016b), Beluga whales in the western Beaufort Sea: Current state of knowledge on timing, distribution, habitat use and environmental drivers, *Deep Sea Res., Part II*, in press.
- Steele, M., S. Dickinson, J. Zhang, and R. Lindsay (2015), Seasonal ice loss in the Beaufort Sea: Toward synchrony and prediction, *J. Geophys. Res. Oceans*, **120**, 1118–1132, doi:10.1002/2014JC010247.
- Thorndike, A. S., and R. Colony (1982), Sea ice motion in response to geostrophic winds, *J. Geophys. Res.*, **87**(C8), 5845–5852, doi:10.1029/JC087iC08p05845.
- von Appen, W., and R. S. Pickart (2012), Two configurations of the western Arctic shelfbreak current in summer, *J. Phys. Oceanogr.*, **42**, 329–351.
- Watanabe, E. (2011), Beaufort shelf break eddies and shelf-basin exchange of Pacific summer water in the western Arctic Ocean detected by satellite and modeling analyses, *J. Geophys. Res.*, **116**, C08034, doi:10.1029/2010JC006259.
- Weingartner, T., K. Aagaard, R. Woodgate, S. Danielson, Y. Sasaki, and D. Cavalieri (2005), Circulation on the north central Chukchi Sea shelf, *Deep Sea Res., Part II*, **52**(24), 3150–3174.
- Williams, W. J., E. C. Carmack, K. Shimada, H. Melling, K. Aagaard, R. W. Macdonald, and R. G. Ingram (2006), Joint effects of wind and ice motion in forcing upwelling in Mackenzie Trough, Beaufort Sea, *Cont. Shelf Res.*, **26**, 2352–2366, doi:10.1016/j.csr.2006.06.012.
- Woodgate, R. A., T. Weingartner, and R. Lindsay (2010), The 2007 Bering Strait oceanic heat flux and anomalous Arctic sea-ice retreat, *Geophys. Res. Lett.*, **37**, L01602, doi:10.1029/2009GL041621.